

The flat bands at the charge neutrality can be described by an effective Hamiltonian [1–4]

$$H_{\text{eff}} = -\gamma_1^{-N+1} \begin{pmatrix} 0 & (v_F p_-)^N \\ (v_F p_+)^N & 0 \end{pmatrix}, \quad (2)$$

which is written in the basis $[\phi_{A_1}, \phi_{B_N}]^T$, that is, involving only the A and B sites of the bottom and top layers, respectively.

This leads to the following energy dispersion [1–4]:

$$\varepsilon_k = \pm \gamma_1^{-N+1} (\hbar v_F k)^N \sim p^N, \quad (3)$$

shown by red lines in Figure 1. However, the effective Hamiltonian 2 is valid only in the interval $]-p_D, +p_D[$, with $p_D = \frac{\gamma_1}{v_F}$ [4]. Outside this interval the surface subbands are no longer flat and the effective approximation diverges drastically as seen in Figure 1.

INELASTIC LIGHT SCATTERING AT ZERO MAGNETIC FIELD

For the sake of completeness here we closely follow Ref. [5] to briefly present the theoretical description of the electronic Raman process. The interaction of the electrons with photons is included in the Hamiltonian (1) by replacing \mathbf{p} by the canonical momentum $\mathbf{\Pi} = \mathbf{p} + \frac{e}{c} \mathbf{A}(\mathbf{r})$ where \mathbf{A} is the vector potential associated with the light field and it is given by

$$\mathbf{A} = \sum_{\mathbf{l}, \mathbf{q}, q_z} \frac{\hbar c}{\sqrt{2\Omega}} \left(\mathbf{l} e^{i(\mathbf{q}\mathbf{r} - \Omega t)/\hbar} b_{\mathbf{l}\mathbf{q}q_z} + h.c. \right). \quad (4)$$

The latter includes the annihilation operator $b_{\mathbf{l}\mathbf{q}q_z}$ for a photon with in-plane momentum \mathbf{q} , energy Ω (which determines its out-of-plane momentum component $q_z = \sqrt{\Omega^2/c^2 - \mathbf{q}^2}$) and polarization \mathbf{l} . Expanding the (full) Hamiltonian up to the second order in the vector potential, we obtain the interaction part

$$H_{\text{int}} = \frac{ev_F}{c} \mathbf{J} \cdot \mathbf{A} + \frac{e^2}{2c^2} \sum_{i,j} \left(\partial_{p_i p_j}^2 H \right) A_i A_j, \quad (5)$$

where $v_F \mathbf{J} = \nabla_{\mathbf{p}} H$ is the current vertex and $\frac{e^2}{2c^2} \left(\partial_{p_i p_j}^2 H \right)$, with $i = \{x, y, z\}$, is the two photon contact interaction tensor [5]. Thus, there are two contributions to the inelastic light scattering amplitude: a one-step process R_ω (contact interaction) and a two-step process R_D involving an intermediate virtual state. The latter consists of an absorption (emission) of a photon with energy $\Omega(\tilde{\Omega})$ transferring an electron with momentum \mathbf{p} from an occupied state in the valence band into a virtual intermediate state, followed by another electron emission (absorption) of the second photon with energy $\tilde{\Omega}(\Omega)$, which moves the electron to the final state with momentum $\mathbf{p} + \mathbf{q} - \tilde{\mathbf{q}}$ and given by [5–7]

$$R_D = \frac{(e\hbar v_F)^2}{2\sqrt{\Omega\tilde{\Omega}}} \left[(\mathbf{J}_{\mathbf{q}} \cdot \mathbf{l}) G_{\Omega+\epsilon_i}^A (\mathbf{J}_{-\tilde{\mathbf{q}}} \cdot \tilde{\mathbf{l}}^*) + (\mathbf{J}_{-\tilde{\mathbf{q}}} \cdot \tilde{\mathbf{l}}^*) G_{-\Omega+\epsilon_f}^A (\mathbf{J}_{\mathbf{q}} \cdot \mathbf{l}) \right]. \quad (6)$$

Here $\mathbf{J}_{\mathbf{q}}$ denotes $\mathbf{J}(\mathbf{q})$ and $G_{\Omega+\epsilon_i}^A$ is the advanced Green function for electrons with energy $\Omega + \epsilon_i$ where ϵ_i correspond to the energy of initial (final) electronic state. The energy difference $\omega = \Omega - \tilde{\Omega} = \epsilon_f - \epsilon_i$ is the Raman shift. The contact interaction process, due to the terms quadratic in the electron momentum \mathbf{p} , is

$$R_\omega = \frac{(e\hbar)^2}{2\sqrt{\Omega\tilde{\Omega}}} \left(\partial_{p_i p_j}^2 H \right) l_i \tilde{l}_j^* \delta_{\mathbf{p}, \mathbf{p} + \mathbf{q} - \tilde{\mathbf{q}}}. \quad (7)$$

In our case, $\mathbf{J} = (\sigma_x \otimes \mathbb{I}, \sigma_y \otimes \mathbb{I}, \sigma_z \otimes \mathbb{I})$ with \mathbb{I} the $N \times N$ identity matrix and σ_i the 2×2 Pauli matrices. Considering $v_F p \ll \Omega$ ($G_{\Omega+\epsilon_i}^A = 1/\Omega$ and $G_{-\Omega+\epsilon_f}^A = -1/\Omega$) the dominant contributions to the Raman scattering amplitude is

$$R_D = \frac{(e\hbar v)^2}{\Omega^2} \left(-i \left(\mathbf{l} \times \tilde{\mathbf{l}}^* \right)_z J_z \right) \quad (8)$$

whereas the contact interaction take the form

$$R_\omega = \frac{(e\hbar v)^2}{6\Omega\gamma_0} (\hat{\epsilon}_z \times \mathbf{J}) \cdot \mathbf{d} \quad (9)$$

with $\mathbf{d} = (l_x \tilde{l}_y^* + l_y \tilde{l}_x^*, l_x \tilde{l}_x^* - l_y \tilde{l}_y^*)$. The transition amplitude $R = R_D + R_\omega$ is analogous to what was obtained for monolayer graphene [6].

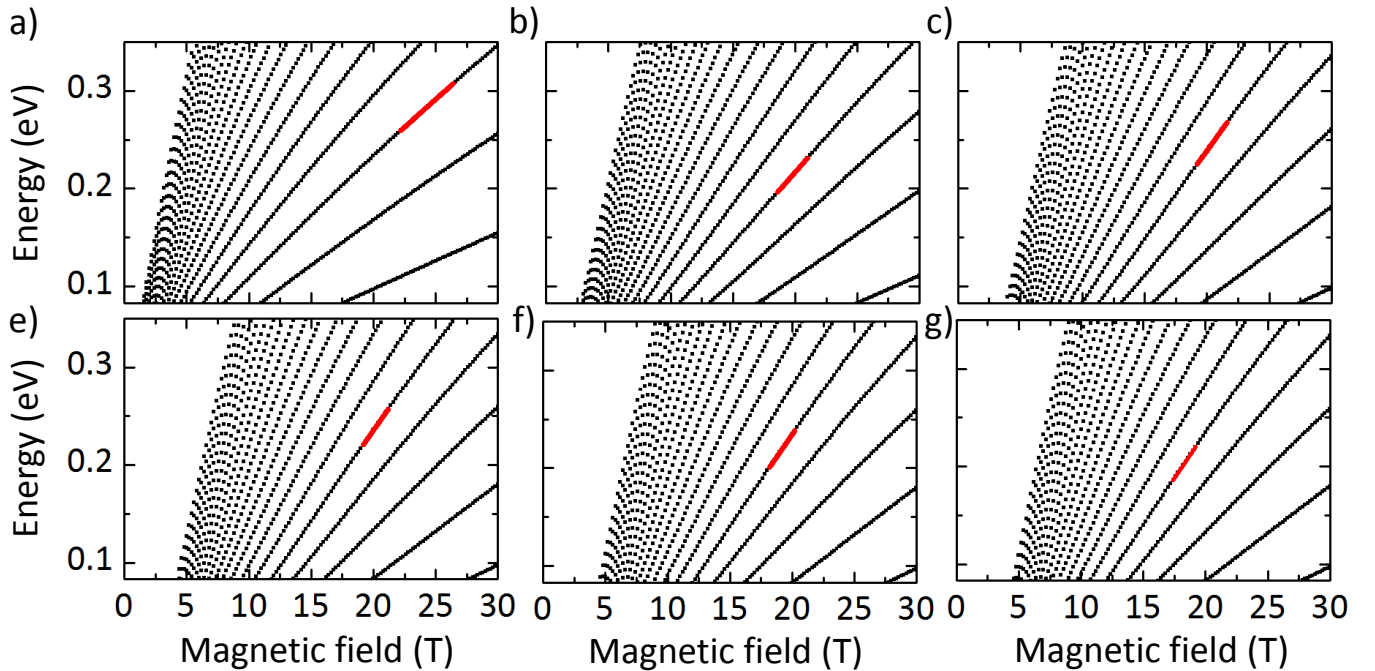


FIG. 2: a-g), Inter-Landau level transitions ($\Delta n = 0$) from the surface subbands, for $N = 3, 8, 10, 14, 17$, respectively. The red line in each plot indicate a linear fitting for a given transition.

equation. For each one of the different form of the eigenstates in Eq. (15) there is always one eigenstate with zero energy while the remaining possible states appear around $\sim \pm\gamma_1$ for small magnetic field. Hence, there are N nontrivial eigenstates with zero energy for ABC-stacked N -layers graphene [1]. Notice that this result can also be obtained from the effective Hamiltonian (2).

To find the electronic Raman spectrum in the presence of an external magnetic field, we calculate transition amplitude (matrix elements of the operator $R = R_D + R_\omega$) between the initial $|\psi_n^\alpha\rangle$ and final $|\psi_m^\beta\rangle$ states. This procedure leads to the selection rules $n = m$ and $\alpha = \beta$ for the R_D process as in monolayer graphene where the ones allowed by R_D correspond to a symmetric optically active inter-LL excitations (transitions with $\Delta n = 0$ in the usual Landau notation for monolayer graphene). Transitions with $m \neq n$ are also possible, due to processes represented by R_ω , but in this case with intensities considerably lower. In order to compare our theoretical calculations with the false color maps of the magneto-Raman scattering spectrum (Figures 4c-d of the main text) we assign a gaussian function to each possible transitions line with height equal to $|\langle\psi_m^\beta|R|\psi_n^\alpha\rangle|^2$ and standard deviation $\sigma \simeq 0.004$ eV to simulate a possible Landau level broadening in the real sample.

LANDAU LEVEL EVOLUTION AS A FUNCTION OF NUMBER OF LAYERS

Figure 2a-g shows a series of plots of the B-evolution of the inter-band Landau level transitions from the surface subbands, for different number of layers N . The slope of these lines increases with the number of layers until reaching a maximum value for the bulk limit. As we discussed in the main text, the evolution of these lines is quasi-linear in the energy range where we performed the magneto-Raman measurements. However, the modeling of these data shows that these lines will depart from the linear regime and ultimately curve at very low energy to reach the zero energy value at $B = 0T$, reproducing the flat part of the surface subband at $B = 0T$ (see Figure 1). From the evolution of the Landau level transitions with the number of layers, we can extract the value of the intercept for each line by performing a linear fitting $A.x + E_0$, where E_0 is the value of the energy at $B = 0T$ obtained from the extrapolation of the Landau level transition lines for a given number of layers N . Figure 3, is a plot of E_0 as a function of N , from 3 to 17 layers. By performing magneto-Raman measurements of the electronic excitations in ABC stacked N -LG, one can estimate the number of layers on the flake from E_0 , by a linear fitting of the B-evolution of the electronic excitations from the surface subbands in the linear regime (i.e., from 600 to 2800 cm^{-1} or from 0.08 to 0.35 eV).

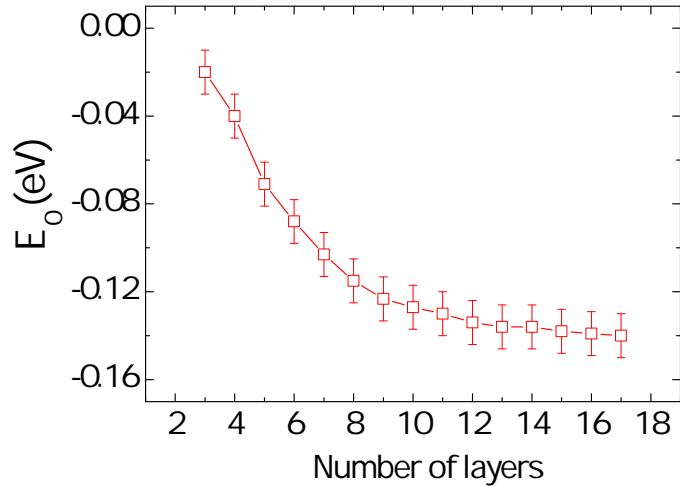


FIG. 3: Evolution of E_0 as a function of N , from 3 to 17 layers. The error bars indicate the uncertainty around the value of E_0 from the fitting of different lines in each plot.

CASE OF MIXED STACKING OF GRAPHENE LAYERS

For the sake of comparison, we also performed magneto-Raman measurements on h2, a region where no ERS at $B = 0$ is observed (boxed region in Figure 4a). A comparison between the observed electronic excitations in h2 and those observed in h3 and h4 is shown in Figure 4b, for different values of the magnetic field, after subtraction of the $B = 0$ spectrum. At first glance, the electronic excitations observed in h2 have rather asymmetric line shapes, if compared to the well symmetric features observed on the ABC stacked suspended parts (h3, h4). The electronic excitation spectrum obtained at h2 is shown in Figure 4c as a false color map of the Raman scattering intensity as a function of the magnetic field. Different electronic excitations are observed, with a quasi linear evolution with increasing magnetic field. The energy of the large majority of these excitations converge to zero when the magnetic field tends to $B = 0$, which is characteristic of the magneto-Raman response of ABA stacked N-LG. Nevertheless, we observe at least three excitations, that extrapolate to a finite B in a similar way to the observed excitations from h3 and h4, reported in the main text. Of much weaker intensity, these three excitations are better seen in the B -differentiated false color map of h2, they are indicated by red arrows in Figure 4d.

In order to illustrate the difference in the dispersion of the electronic excitations with magnetic field between h2 (where the ABA stacking dominates) and h3 or h4 (where there is pure ABC stacking), we performed a spatial mapping of our N-LG flake at fixed magnetic field $B = 17$ T. Figure 5a shows two Raman spectra taken from this map at h2 (red curve) and h4 (black curve). These two Raman spectra show an electronic excitation at different energies, hence the two suspended parts have distinct electronic excitations spectra. The false color map in Figure 5b is obtained by plotting the Raman scattering intensity of the difference in the electronic excitation dispersion all over the flake. From the conspicuous contrast in Figure 5b, we reveal again, thanks to magneto-Raman spectroscopy, the two domains with different stacking configurations.

The evolution with magnetic field of the electronic excitations in h2 can be understood by considering a tight-binding model for N-LG system with a mixed stacking of its graphene layers. In this case, the Hamiltonian contains an ABA-stacked 8 layers graphene coupled to 7 layers with an ABC sequence. The low energy electronic band structure corresponding to the ABABABAB-ABCABCA stacked 15-LG is shown in Figure 6a. The best fit for h2 yields $N = 15$ with $\gamma_0 = 3.15$ eV and $\gamma_1 = 0.4$ eV (Figure 6b-c). Where the three excitations observed in h2 that extrapolate at finite $B = 0$ originate from the symmetric (i.e., $\Delta|n| = 0$) inter-band Landau level transitions within the flat bands at the charge neutrality in Figure 6a. While the almost parabolic bands in Figure 6a give rise to the remaining complex electronic excitations spectrum observed in h2. The main conclusion is that while the suspended parts h3 and h4 that have been discussed in the main text, have a rather pure ABC stacking, h2 on the other hand is interpreted as being inhomogeneous and exhibits both ABA and ABC stacking configurations. It is interesting to emphasize the striking difference in complexity that both cases present, while the mixed stacking case (h2) presents a rather complicated magneto-Raman spectrum, the pure ABC stacking situation (h3 and h4) shows a clean and simple one.

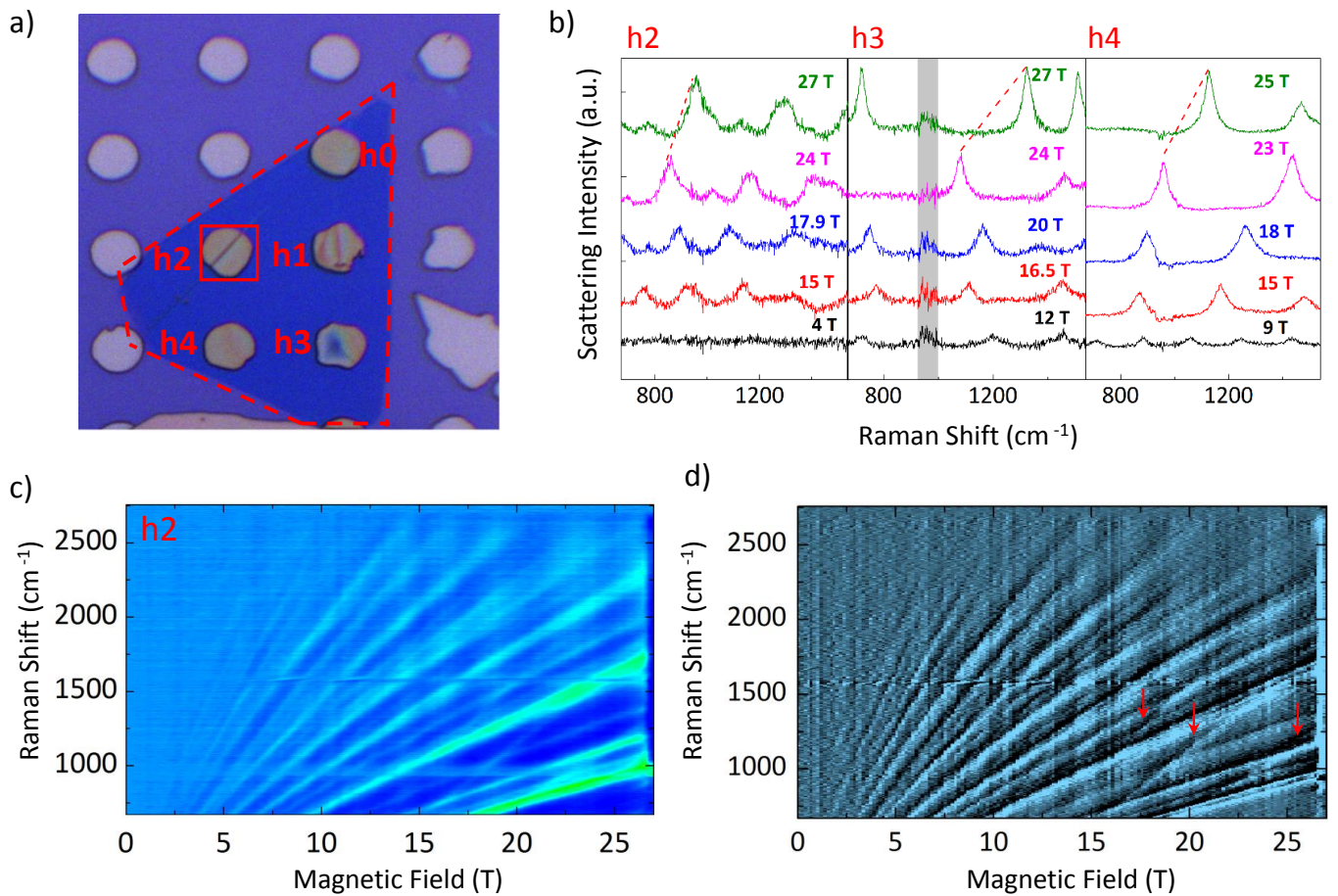


FIG. 4: **Observation of low temperature electronic excitations from N-LG with a mixed stacking of graphene layers.** a), Optical microscope image of the N-LG, the suspended part where magnetic dependent magneto-Raman spectra have been recorded, labelled h2, is boxed in red square. b), $B = 0$ subtracted Raman spectra from h2, and the previously measured h3, and h4 respectively, for different values of the magnetic field. c), False color map of the micro-Raman scattering intensity spectra as function of magnetic field from h2. d), B -differentiated false color map of (b), the three excitations that extrapolate at finite B are indicated by red arrows.

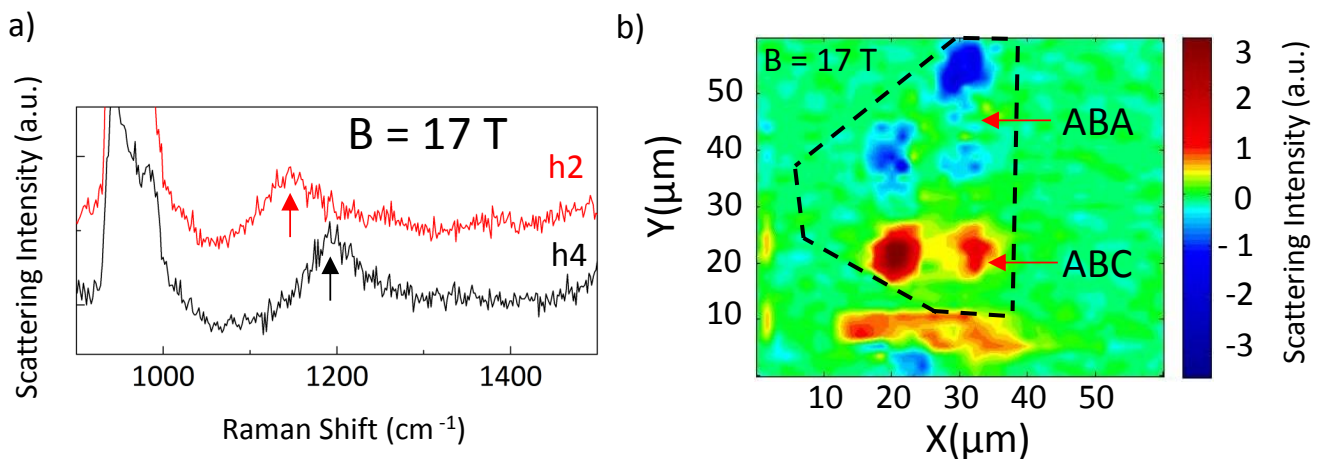


FIG. 5: **Contrast in electronic excitations spectrum from the two domains.** Raman spectra recorded at $B = 17$ T from h2 and h4. The contrast in the scattering intensity between the two domains is shown in (b) in the form of a false color map of the micro-Raman scattering intensity from the N-LG flake at $B = 17$ T, showing the contrast in the Raman scattering intensity as a function of the stacking configuration (i.e., ABA or ABC).

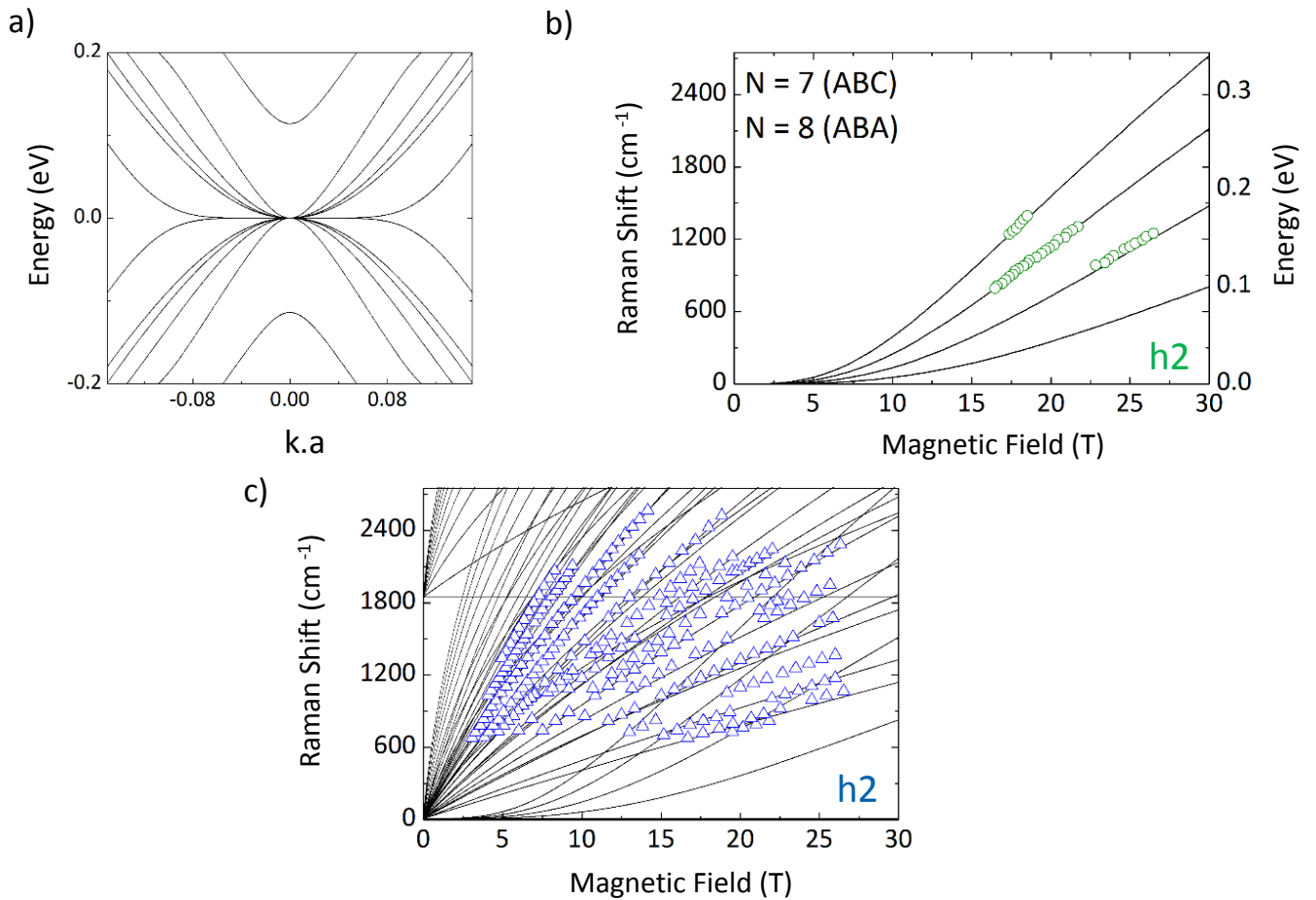


FIG. 6: **Modeling of the data from the magneto-Raman experiment on h2.** By considering a single tight-binding Hamiltonian that contains the stacking configuration ABABABAB-ABCABCA, we plot its low energy band structure in (a). The fitting of the electronic excitations observed in h2 is obtained by considering the symmetric inter Landau level transitions of an ABC stacked 7 layer graphene, indicated by green colored data in (b), coupled with an ABA stacked 8 layer graphene, indicated by blue colored data in (c).

ATOMIC FORCE MICROSCOPY MEASUREMENTS

To investigate the thickness of the flake, we performed atomic force microscopy (AFM) on three different edges as seen in Figure 7a. The thickness was estimated from the edges by assuming a thickness for the first monolayer sheet on top of the silicon dioxide layer equal to 0.529 nm (as measured under nominally the same conditions for a reference graphene flake). The atomic interlayer distance in graphite is taken to be 0.335 nm, this gives a thickness that varies from 15 to 17 layers, in accordance with the number of layers we used in the tight binding model to fit the experimental data.

* Electronic address: marek.potemski@lncmi.cnrs.fr

† Electronic address: clement.faugeras@lncmi.cnrs.fr

- [1] H. Min and A. H. MacDonald, Phys. Rev. B **77**, 155416 (2008), URL <http://link.aps.org/doi/10.1103/PhysRevB.77.155416>.
- [2] M. Koshino and E. McCann, Physical Review B **80**, 165409 (2009).
- [3] F. Zhang, B. Sahu, H. Min, and A. H. MacDonald, Phys. Rev. B **82**, 035409 (2010).
- [4] C.-H. Ho, C.-P. Chang, and M.-F. Lin, Phys. Rev. B (2016).
- [5] O. Kashuba and V. I. Falko, New J Physics **14**, 105016 (2012), URL <http://iopscience.iop.org/article/10.1088/>

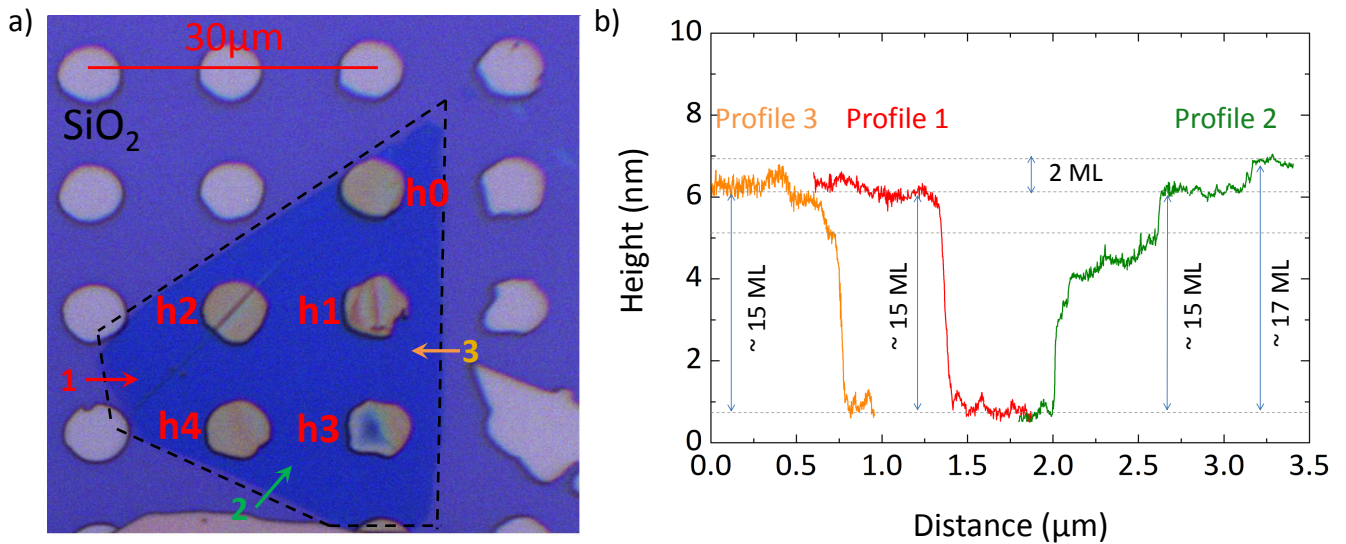


FIG. 7: a), Optical microscope image of the flake, the colored arrows indicate the sections where AFM measurements were performed. b), Plot of the edges profile (a) obtained from the AFM. The thickness varies from 15 to 17 graphene monolayers.

1367-2630/14/10/105016/meta;jsessionid=A7ACD5736913C507330CAE633641119F.c1.iopscience.cld.iop.org.

- [6] O. Kashuba and V. I. Fal'ko, Phys. Rev. B **80**, 241404 (2009), URL <http://link.aps.org/doi/10.1103/PhysRevB.80.241404>.
- [7] M. Mucha-Kruczyński, O. Kashuba, and V. I. Fal'ko, Phys. Rev. B **82**, 045405 (2010), URL <http://link.aps.org/doi/10.1103/PhysRevB.82.045405>.
- [8] S. Yuan, R. Roldán, and M. I. Katsnelson, Phys. Rev. B **84**, 125455 (2011), URL <http://link.aps.org/doi/10.1103/PhysRevB.84.125455>.